Available online at www.sciencedirect.com
ScienceDirect
Journal of Power Sources 181 (2008) 199–206
JOURNAL OF POWER SOURCES
www.elsevier.com/locate/jpowsour

The effect of co-dopant addition on the properties of $Ln_{0.2}Ce_{0.8}O_{2-\delta}$ (Ln = Gd, Sm, La) solid-state electrolyte

E.Yu. Pikalova [a], V.I. Maragou [b], A.N. Demina [a], A.K. Demin [a,**], P.E. Tsiakaras [b,*]

[a] *Institute of High Temperature Electrochemistry, 22 S. Kovalevskoy, 620219 Ekaterinburg, Russia*
[b] *School of Engineering, Department of Mechanical Engineering, University of Thessaly, Pedion Areos, 383 34 Volos, Greece*

Received 28 September 2007; received in revised form 31 January 2008; accepted 1 February 2008
Available online 12 February 2008

Abstract

The present work aims at the investigation of $Ln_{0.2}Ce_{0.8}O_{2-\delta}$ (where Ln = Sm, La, Gd) structural and electrical properties when in the Ln sub-lattice, Ba^{2+} and Sr^{2+} with ionic radii 1.42 and 1.26 Å, respectively, are introduced. The conductivity measurements were held both in air and in $H_2 + 3\%H_2O$ atmosphere using the 4-probe dc technique at the temperature range of 600–900 °C. Among all the samples, the highest value of electrical conductivity is obtained in the case of $(Sm_{0.75}Sr_{0.2}Ba_{0.05})_{0.2}Ce_{0.8}O_{2-\delta}$, both in air and in hydrogen atmosphere. In the case of $H_2 + 3\%H_2O$ the conductivity of the co-doped compounds increases in comparison with air. Moreover, the dependence of conductivity on the oxygen partial pressure, measured at the P_{O_2} range of 0.21–10^{-22} atm, showed that the electrolytic area of alkaline-earth metals doped $Ln_{0.2}Ce_{0.8}O_{2-\delta}$ is considerably enhanced, as predicted by the theory. Finally, by comparing the thermal expansion coefficients of the different materials (TEC), the thermo-mechanical compatibility between the co-doped and the other cell components was also investigated.

Keywords: Doped ceria; Electrical conductivity; Thermal expansion coefficient; Co-dopant

1. Introduction

It is well known that oxygen ion conductors constitute materials of special interest, due to the fact that they are used in many applications, such as oxygen sensors, electrochemical oxygen pumps and solid oxide fuel cells (SOFCs). In the case of SOFCs systems, electrolytes' high oxide ionic conductivity is requisite for high electrical power generation. The most commonly used electrolyte, yttria stabilized zirconia, exhibits sufficient ionic conductivity at ∼1000 °C and is characterized by good thermal stability. On the other hand, ceria solid solutions exhibit 4–5 times higher ionic conductivity values at the intermediate temperature range [1]. This property has provoked the increasing interest of the scientific community on the investigation and the use of ceria as the electrolytic material, since the reduction of the operation temperature of SOFCs, constitutes a primary goal that has to be reached. SOFCs operation at intermediate temperature values (600–800 °C) provides several advantages since it: (i) enables the use of inexpensive materials as interconnects, (ii) enhances the stability and the durability of all the components and (iii) offers the potential of more rapid start up and shut down procedures [2].

However, at low oxygen partial pressures these materials are partially reduced because of the reduction of Ce^{4+} to Ce^{3+} [1]. Additionally, when exposed to the reducing atmosphere of the fuel cell anode, the singly doped material develops electronic conductivity as well, resulting in efficiency loss. Considerable efforts towards the reduction of the electronic conductivity of ceria-based electrolytes have already been made. For example, Maricle et al. [3] reported that the addition of 3 mol% of praseodymium to gadolinia-doped ceria (CGO) decreases by two orders of magnitude (3.7×10^{-21} atm at 700 °C) the electrolytic domain boundary, which is defined as the partial pressure of oxygen below which the electronic conductivity exceeds the ionic conductivity. Kim et al. [4] added separately five trivalent metal (Y, Sm, Nd, Pr and La) oxides, prepared by the Pechini method, up to 5 mol% as a co-dopant to 20 mol% CGO. It was found that only samaria and yttria increase the electrical conductivity of the electrolyte and the maximum value at 700 °C was reached in the case of Sm at 3 mol% (6.4×10^{-2} S cm^{-1}

* Corresponding author. Tel.: +30 24210 74065; fax: +30 24210 74050.
** Co-corresponding author. Tel.: +7 3432 745431; fax: +7 3432 745992.
E-mail addresses: A.Demin@ihte.uran.ru (A.K. Demin), tsiak@uth.gr (P.E. Tsiakaras).

0378-7753/$ – see front matter © 2008 Elsevier B.V. All rights reserved.
doi:10.1016/j.jpowsour.2008.02.003

for doped 3 mol% Sm CGO20 and 4.75×10^{-2} S cm^{-1} for undoped one).

Mori et al. investigated the improvement of CeO_2-based oxides from the viewpoint of crystallography [5,6]. They assumed that the reduction of Ce^{4+} in a fluorite lattice is inhibited by the expansion of CeO_2 lattice. The ionic radii of Ce^{4+} and Ce^{3+} in CeO_2 are 0.97 and 1.14 Å, respectively [7]. Consequently, the authors made the assumption that the fluorite lattice of CeO_2 receives dopants which have an average ionic radius up to 1.14 Å. It was found that small amounts of Ca or Cs (ionic radii 1.12 and 1.74 Å, respectively) doped in CeO_2–Sm_2O_3 system, prepared by the co-precipitation method, show high oxide ionic conductivity (4.56×10^{-2} S cm^{-1} for $Sm_{0.25}Ce_{0.75}O_{2-\delta}$, 10.95×10^{-2} S cm^{-1} for $(Sm_{0.5}Ca_{0.5})_{0.25}Ce_{0.7}O_{2-\delta}$ and 18.56×10^{-2} S cm^{-1} for $(Sm_{0.936}Cs_{0.06}Li_{0.004})_{0.25}Ce_{0.75}O_{2-\delta}$ at 800 °C). Moreover, these samples were found to be quite effective in suppressing the reduction of CeO_2 by measuring the electrical conductivity as a function of oxygen partial pressure. At 800 °C the electrical conductivity of $Sm_{0.25}Ce_{0.75}O_{2-\delta}$ was constant up to an oxygen partial pressure close to 10^{-6} atm, while the values of electrical conductivity of $(Sm_{0.5}Ca_{0.5})_{0.25}Ce_{0.75}O_{2-\delta}$ and $(Sm_{0.936}Cs_{0.06}Li_{0.004})_{0.25}Ce_{0.75}O_{2-\delta}$ were constant at oxygen partial pressures up to 10^{-8} and 10^{-11} atm, respectively, leading to the conclusion that the expansion of the fluorite lattice increases the reduction resistance of CeO_2–Sm_2O_3 [6]. Because of the high oxide ionic conductivity and the good reduction resistance, the maximum power density of $(Sm_{0.936}Cs_{0.06}Li_{0.004})_{0.25}Ce_{0.75}O_{2-\delta}$ reached the value of 0.85 W cm^{-2} at 1000 °C, which was about three times higher than that of $Sm_{0.25}Ce_{0.75}O_{2-\delta}$ [6]. The ionic conductivity of $(La_{0.75}Sr_{0.2}Ba_{0.05})_{0.175}Ce_{0.825}O_{1.891}$, prepared by the co-precipitation method, was constant up to 10^{-16} atm, suggesting that the ionic domain of the doped CeO_2-based material with high suggested index was apparently expanded by the enhancement of ionic conductivity [5].

Taking into account that Sm, Gd and La-doped CeO_2 are considered to be promising solid-state electrolyte materials [1], the aim of the present work is to check their electrolytic properties during the introduction of Ba^{2+} and Sr^{2+} with ionic radii 1.42 and 1.26 Å, respectively, into the sublattice of Ln (Ln = Sm, La, Gd). In order to examine the dependence of the electrical properties of the above mentioned electrolytes on the average ionic radius, in the present work the latter were calculated by the following equation for $(Ln_{0.75}Sr_{0.2}Ba_{0.05})_{0.2}Ce_{0.8}O_{2-\delta}$:

$$(X\ \text{Å} \times 0.75) + (1.26\ \text{Å} \times 0.2) + (1.42\ \text{Å} \times 0.05) = \text{average ionic radius Å} \quad (1)$$

where X denotes the ionic radius of the rare-earth element. For Ln = Sm, La, Gd the values of the average ionic radius were 1.1405, 1.208 and 1.118 Å, respectively.

The reduction of Ce^{4+} to Ce^{3+} leads to the volume expansion of the CeO_2 lattice. In the present work it was assumed that if the lattice of CeO_2-based oxide is previously expanded by the dissolution of Ba^{2+} and Sr^{2+} in it, such lattice expansion would inhibit its further volume expansion under reducing conditions. Kilner [8] has pointed out that the minimum value of activation energy for conduction is reached when the ionic radii of the host and the dopant are close to each other, because in this case the lattice elastic strain is minimized. Since $(Sm_{0.75}Sr_{0.2}Ba_{0.05})$ has the same value as Ce^{3+}, it is expected that it will exhibit the best electrolytic properties among the investigated compounds under reducing conditions.

2. Experimental

The solid-state compositions of $Ln_{0.2}Ce_{0.8}O_{2-\delta}$ and $(Ln_{0.75}Sr_{0.2}Ba_{0.05})_{0.2}Ce_{0.8}O_{2-\delta}$ (with Ln = Sm, Gd, La) were synthesized via a solid-state reaction from CeO_2, Gd_2O_3, Ln_2O_3, Sm_2O_3 oxides and $SrCO_3$,$BaCO_3$ carbonates of high purity. The main component content in the materials used for synthesis was no less then 99.99%. The powders were weighed according to the stoichiometry and ball milled in ethyl alcohol medium for 0.5 h in a plastic bottle using zirconia balls in the planetary mill FRITSCH pulverisette-6. The sintering involved several stages. First, the mixtures were held at 950 °C for 10 h in order to remove carbon dioxide; then the reaction masses were cooled, ground for 2 h and sintered again at 1050 °C for 10 h. The substances thus obtained were ground for 2 h. The powder mixtures were calcined at 1300 °C for 10 h and then ball milled for 2 h again. The specific surface area, tested by particle size analyzer SA-CP2 Shimadzu, was approximately 3.3842 m^2 g^{-1}. The samples were prepared in the form of sheets by rolling with the addition of 5% solution of natural rubber in a mixture of acetone and gasoline (60/40). The samples of 20 mm × 5 mm × 1 mm size were cut from the sheets and calcined for the elimination of the organic binders at 500 °C for 30 h with a heating/cooling rate of 30 °C h^{-1}. Then the $Ln_{0.2}Ce_{0.8}O_{2-\delta}$ samples were sintered at 1700 °C, while the $(Ln_{0.75}Sr_{0.2}Ba_{0.05})_{0.2}Ce_{0.8}O_{2-\delta}$ samples at 1580 °C for 3 h in air, with a heating/cooling rate of 180 °C h^{-1}.

The density of the sintered samples was measured by employing both the Archimedes principle and the calculation from the weight and the dimensions of the specimens. It was found that both methods of obtaining the density provided almost the same value. The average value derived from the two methods for each specimen was compared to the theoretical one, calculated from the lattice parameters.

The X-ray diffraction (XRD) technique was employed to identify the phases and to obtain the values of the lattice constants. The XRD analysis was performed on the milled powders of specimens by using a DMAX-2500, Rigaku Co. Ltd., Japan diffractometer with Ni-filtered Cu Kα radiation in the range of $10^\circ \le 2\theta \le 120^\circ$. The unit cell parameters of the samples were refined using the Rietveld profile analysis method with the Fullprof program (sp. gr. *Fm3m*) [9]. The main idea of the method is that the calculated diffractogramm is compared with the experimental one. By this comparison the profile (half-widths, diffractogramm shear, unit cell parameters, asymmetry parameters, scale coefficient, profile parameter, background coefficient and heat factor) and the structural parameters (atoms coordinates, individual isotropic or anisotropic heat factors) are refined.

The criteria of refinement quality are the following R-factors:

$$\text{profile, } R_{\mathrm{p}} = \frac{\sum |y_{\mathrm{ie}} - k y_{\mathrm{ie}}|}{\sum y_{\mathrm{ie}}} \tag{2a}$$

$$\text{weight profile, } R_{\mathrm{wp}} = \left(\frac{\sum w_{\mathrm{i}} (y_{\mathrm{ie}} - k y_{\mathrm{it}})^2}{\sum w_{\mathrm{i}} y_{\mathrm{ie}}^2} \right)^{1/2} \tag{2b}$$

$$\text{Bragg-factor, } R_{\mathrm{Br}} = \frac{\sum |I_{\mathrm{it}} - c I_{\mathrm{kt}}|}{\sum I_{\mathrm{ke}}} \tag{2c}$$

$$\text{structural, } R_{\mathrm{f}} = \frac{\sum |F_{\mathrm{it}} - c F_{\mathrm{kt}}|}{\sum F_{\mathrm{ke}}} \tag{2d}$$

$$\text{expected, } R_{\mathrm{exp}} = \left\{ \frac{N - P}{\sum w_{\mathrm{i}},\, y_{\mathrm{ie}}^2} \right\}^{1/2} \tag{2e}$$

where y_{ie}, y_{it}, denote the experimental and theoretical intensities on each angle; I_{it}, I_{kt} the experimental and theoretical integral reflexes intensities; F_{it}, F_{kt} the experimental and theoretical structural amplitudes; k, c are the scale multipliers; N the experimental points number; P the refined parameters number; and $w_{\mathrm{i}} = 1/y_{\mathrm{ie}}$ the weight multipliers.

The angle halfwidth dependence is written as

$$H_k^2 = U \operatorname{tg}^2 \theta + V \operatorname{tg} \theta + W \tag{3}$$

where θ is the dispersion angle and H_k the full width on the half of the maximum of k-Bragg reflex. The crystal structure refinement was held by Rietveld method by using the profile of Pseudo-Voit function.

The electrical conductivity measurements of the samples were carried out by employing the four-point dc technique in different atmospheres. The experimental apparatus is cited in Fig. 1. The specimens were installed in a tube made from ZrO_2-based electrolyte. The flowrate of the gas mixtures into the outer and the inner space of the YSZ tube was adjusted by digital mass flow controllers (Brooks Series 5800) at 20 ml min^{-1}. Platinum paste stripes, which were deposited on the inner and outer surface of the YSZ tube and connected with platinum wires, were used as the electrochemical oxygen pump and the oxygen sensor. On the samples' surface four Pt electrodes were deposited on and connected with Pt wires. The one pair was used in order to apply voltage (50–1000 mV) with an electrochemical station (Amel Instruments Model 2053). The second pair of electrodes was connected to a multimeter in order to register the voltage of the samples. The atmospheres with various oxygen partial pressures inside the tube were created by means of oxygen pumping and registered by the aid of the sensor. Temperature and oxygen partial pressure were varied automatically by means of microprocessor system Zirkonia-318 in the range of 600–900 °C and 0.21–10^{-22} atm, respectively.

Finally, the thermal expansion of the samples was measured using an AF-1 dilatometer during heating/cooling with a rate of 200 °C h^{-1} from room temperature to 900 °C and vice versa, and exposure at each point for 20 min every 50 °C.

3. Results and discussion

3.1. X-ray diffraction analysis

Table 1 summarizes the experimental results of the XRD analysis. As it can be seen all samples consisted of fluorite solid solutions. No other phases were observed. The incorporation of rare-earth ions (La^{3+}, Sm^{3+}, Gd^{3+}) into the lattice of CeO_2 leads to the increase of both the cubic structure parameters and the volume of the elementary cells of $La_{0.2}Ce_{0.8}O_{2-\delta}$, $Sm_{0.2}Ce_{0.8}O_{2-\delta}$ and $Gd_{0.2}Ce_{0.8}O_{2-\delta}$. The dependence on the variation of cell parameters is probably conditioned by the decrease of ionic radii: 1.18, 1.09, 1.06, 0.97 Å in row La_{VIII}^{3+}, Sm_{VIII}^{3+}, Gd_{VIII}^{3+}, Ce_{VIII}^{4+}, respectively [7].

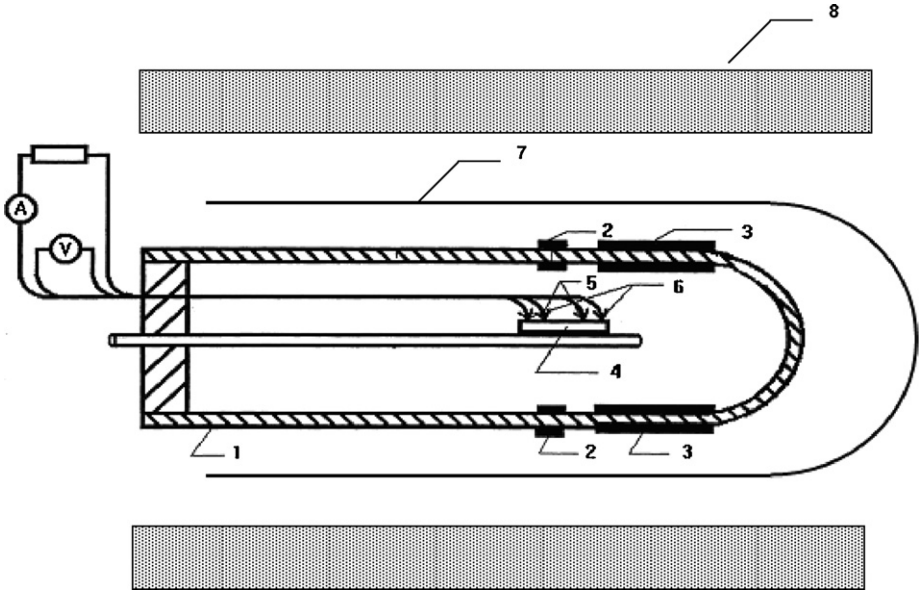

Fig. 1. (1) YSZ tube, (2) sensor electrode, (3) pump electrode, (4) sample, (5) potential probes, (6) current probes, (7) quartz tube, and (8) furnace.

Table 1
Parameters of elementary cells of un-doped and doped CeO_2

Composition	a (Å)	V (Å^3)	R_{Br}	R_f	ρ_T, (g cm^{-3})	$\rho_{sam.}$ (%) of ρ_T
CeO_2	5.4099(2)	158.33	1.04	0.695	7.22	97
$La_{0.2}Ce_{0.8}O_{2-\delta}$	5.4720(3)	163.85	1.324	1.060	6.87	68
$Sm_{0.2}Ce_{0.8}O_{2-\delta}$	5.4300(2)	160.10	1.29	0.735	7.12	83
$Gd_{0.2}Ce_{0.8}O_{2-\delta}$	5.4219(2)	159.39	0.959	0.607	7.21	93
$(La_{0.75}Sr_{0.2}Ba_{0.05})_{0.2}Ce_{0.8}O_{2-\delta}$	5.4636(2)	163.10	0.718	0.569	7.05	91
$(Sm_{0.75}Sr_{0.2}Ba_{0.05})_{0.2}Ce_{0.8}O_{2-\delta}$	5.4353(2)	160.57	0.675	0.569	7.23	88
$(Gd_{0.75}Sr_{0.2}Ba_{0.05})_{0.2}Ce_{0.8}O_{2-\delta}$	5.4299(2)	160.10	0.767	0.540	7.29	86

The introduction of alkaline-earth metals into the lattice of $La_{0.2}Ce_{0.8}O_{2-\delta}$, $Sm_{0.2}Ce_{0.8}O_{2-\delta}$ and $Gd_{0.2}Ce_{0.8}O_{2-\delta}$ provides the possibility of sintering $(La_{0.75}Sr_{0.2}Ba_{0.05})_{0.2}Ce_{0.8}O_{2-\delta}$, $(Sm_{0.75}Sr_{0.2}Ba_{0.05})_{0.2}Ce_{0.8}O_{2-\delta}$ and $(Gd_{0.75}Sr_{0.2}Ba_{0.05})_{0.2}Ce_{0.8}O_{2-\delta}$ single phase compositions at lower temperatures. The corresponding XRD patterns are shown in Fig. 2. All these compounds are isostructural to the un-doped CeO_2 and present perfect cubic structure. The increase of the elementary cell parameters of the alkaline-earth metals doped compounds are justified by the effect on the dimensions when La^{3+}, Sm^{3+} and Gd^{3+} are substituted by the bigger ions of Sr^{2+} ($r = 1.25$ Å) and Ba^{2+} ($r = 1.42$ Å).

The theoretical (calculated from the volume of the elementary cell) and relative densities of the sintered bodies (1700 °C for un-doped and 1580 °C for doped with Ba and Sr), ρ_T and $\rho_{sam.}$, respectively, are presented in Table 1. As one can observe the sintering properties of $La_{0.2}Ce_{0.8}O_{2-\delta}$ are not satisfying enough (the relative density is 68% at sintering temperature 1700 °C). The introduction of alkaline-earth metals improves the sintering properties and relative density of $(La_{0.75}Sr_{0.2}Ba_{0.05})_{0.2}Ce_{0.8}O_{2-\delta}$ which increases up to 91% at lower temperature (1580 °C). Taking into account that un-doped and doped with Gd and Sm samples prepared at different sintering temperatures have almost the same value of relative density, one could conclude that the introduction of alkaline-earth metals improves the sintering properties of electrolytes on a base of CeO_2.

The thermal expansion coefficients (TEC) for these materials at different temperatures calculated from the present work, as well as the ones from literature [10–14] are cited in Table 2. The thermal expansion coefficient values are mean values that are given for a certain temperature range in which the thermal expansion coefficient changes almost linearly with temperature. The exact value of the thermal expansion coefficient depends strongly on the stoichiometry and the fabrication method of the composition, as well as on the set-up of the thermal expansion measurement. In the present work each thermal expansion coefficient was calculated from the linear dependence of each sample's expansion during the decrease of temperature from 900 to 350 °C, according to the following formula:

$$\alpha_{T_1-T_2} = \frac{\Delta L}{L_0 \times (T_1 - T_2)} \quad (4)$$

where $\alpha_{T_1-T_2}$ denotes the average value of TEC in the temperature interval T_1–T_2, L_0 is the initial length of the sample and ΔL the change of the sample's length in the temperature interval T_1–T_2. As can someone observe, it is obvious that the introduction of alkaline-earth metals into the lattice of $Ln_{0.2}Ce_{0.8}O_{2-\delta}$ (where Ln = Gd, Sm, La) does not change significantly the TEC.

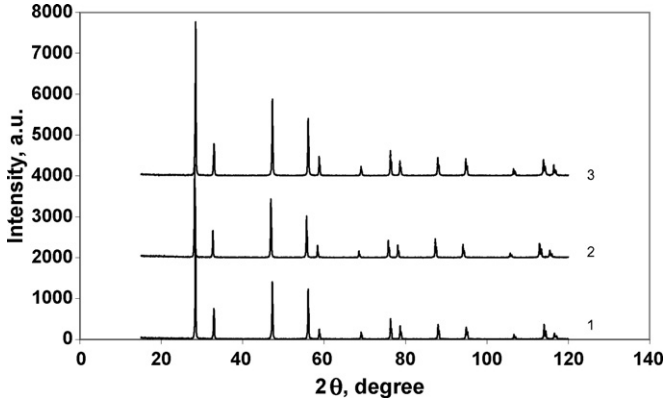

Fig. 2. X-ray diffraction patterns of: (1) $(La_{0.75}Sr_{0.2}Ba_{0.05})_{0.2}Ce_{0.8}O_{2-\delta}$, (2) $(Sm_{0.75}Sr_{0.2}Ba_{0.05})_{0.2}Ce_{0.8}O_{2-\delta}$, and (3) $(Gd_{0.75}Sr_{0.2}Ba_{0.05})_{0.2}Ce_{0.8}O_{2-\delta}$.

3.2. Conductivity measurements

The electrical conductivity of the samples at three different temperatures, as well as the calculated values of activation energy for conductivity, in air and in $H_2 + 3\%H_2O$ atmosphere are presented in Tables 3 and 4, respectively. The values of total conductivity σ_{tot} in air are in a good agreement with the ones obtained for samples prepared via solid-state reactions [15], but significantly lower in comparison with the ones obtained for nano-structure samples prepared via the co-precipitation method [5]. The introduction of alkaline-earth metals increases samples' conductivity almost by 2 times, decreasing at the same time significantly the activation energy of total conductivity. More precisely, for the samples doped with La, Sm and Gd the conductivity increased by 90, 54 and 79% at 800 °C, respectively. The same effect was observed by Mori et al. [5] and Mori and Yamamura [6]. They observed enhancement of electrical conductivity in air for $Sm_{0.25}Ce_{0.75}O_{2-\delta}$ doped with Cs, Li and Ca and $La_{0.175}Ce_{0.825}O_{2-\delta}$ doped with Sr and Ba, prepared via the co-precipitation method (0.046, 0.186, 0.11 and 0.1, 0.56 S cm^{-1} at 800 °C, respectively). Since the ionic transport numbers of oxygen for these samples almost reach unity from 700 to 1000 °C [6] and are independent of temperature, it is concluded that the increase of total electrical conductivity in air can be attributed to the increase of the oxide ionic conduc-

Table 2
Values of thermal expansion coefficient for un-doped and doped CeO_2

Composition	Temperature range (°C)	$\alpha \times 10^6\ K^{-1}$	References
$Gd_{0.2}Ce_{0.8}O_{2-\delta}$	500	12.5	[10]
$Gd_{0.2}Ce_{0.8}O_{2-\delta}$	300–1100	11.8	[11]
$Gd_{0.2}Ce_{0.8}O_{2-\delta}$	50–1000	12.5	[11]
$Gd_{0.2}Ce_{0.8}O_{2-\delta}$	50–900	12.9	[12]
$Gd_{0.2}Ce_{0.8}O_{2-\delta}$	350–900	12.0	Present work
$Sm_{0.2}Ce_{0.8}O_{2-\delta}$	50–900	13.3	[12]
$Sm_{0.2}Ce_{0.8}O_{2-\delta}$	50–500	11.4	[13]
$Sm_{0.2}Ce_{0.8}O_{2-\delta}$	350–900	12.3	Present work
$La_{0.2}Ce_{0.8}0_{2-\delta}$	50–600	11.8	[13]
$La_{0.2}Ce_{0.8}0_{2-\delta}$	50–500	11.7	[14]
$La_{0.2}Ce_{0.8}0_{2-\delta}$	350–900	12.2	Present work
$(La_{0.75}Sr_{0.2}Ba_{0.05})_{0.2}Ce_{0.8}O_{2-\delta}$	350–900	12.8	Present work
$(Sm_{0.75}Sr_{0.2}Ba_{0.05})_{0.2}Ce_{0.8}O_{2-\delta}$	350–900	12.3	Present work
$(Gd_{0.75}Sr_{0.2}Ba_{0.05})_{0.2}Ce_{0.8}O_{2-\delta}$	350–900	12.8	Present work

Table 3
Electrical conductivity of $Ln_{0.2}Ce_{0.8}O_{2-\delta}$ and $(Ln_{0.75}Sr_{0.2}Ba_{0.05})_{0.2}Ce_{0.8}O_{2-\delta}$ (where Ln = Sm, Gd, La) in air at 700, 800 and 900 °C and the calculated E_a values of total conductivity (in the temperature range of 600–900 °C)

Composition	Air, σ_{tot} (S cm^{-1}) 700 °C	Air, σ_{tot} (S cm^{-1}) 800 °C	Air, σ_{tot} (S cm^{-1}) 900 °C	Air, E_a (kJ mol^{-1})
$La_{0.2}Ce_{0.8}O_{2-\delta}$	0.021	0.040	0.072	62
$La_{0.2}Ce_{0.8}O_{2-\delta}$ [15]		0.041		
$La_{0.15}Ce_{0.85}O_{1.925}$ [5]		0.234		
$Sm_{0.2}Ce_{0.8}O_{2-\delta}$	0.024	0.054	0.107	76
$Sm_{0.2}Ce_{0.8}O_{2-\delta}$ [15]	0.049	0.093	0.145	
$Sm_{0.2}Ce_{0.8}O_{2-\delta}$ [5]		0.040		
$Gd_{0.2}Ce_{0.8}O_{2-\delta}$	0.015	0.038	0.062	83
$Gd_{0.2}Ce_{0.8}O_{2-\delta}$ [15]	0.021	0.075	0.123	
$Gd_{0.2}Ce_{0.8}O_{2-\delta}$ [3]	0.028			
$(La_{0.75}Sr_{0.2}Ba_{0.05})_{0.2}Ce_{0.8}O_{2-\delta}$	0.037	0.076	0.124	58
$(La_{0.77}Sr0.2Ba_{0.03})_{0.175}Ce_{0.85}O_{1.892}$ [5]		0.335		
$(Sm_{0.75}Sr_{0.2}Ba_{0.05})_{0.2}Ce_{0.8}O_{2-\delta}$	0.038	0.083	0.152	64
$(Gd_{0.75}Sr_{0.2}Ba_{0.05})_{0.2}Ce_{0.8}O_{2-\delta}$	0.029	0.068	0.126	74

tivity σ_i. In turn the enhancement of ionic conductivity can be attributed to the expansion of the lattice, due to the dissolution of the additives in the fluorite structure. Among all the samples, the highest value of electrical conductivity was registered in the case of $(Sm_{0.75}Sr_{0.2}Ba_{0.05})_{0.2}Ce_{0.8}O_{2-\delta}$, both in air and in hydrogen atmosphere.

When the samples were exposed at $H_2 + 3\%H_2O$ gas mixture, the conductivity of all compounds increased in comparison with air and the activation energy for conduction decreased significantly. It was found that the difference between electrical conductivity in air and hydrogen decreases in the case of $(Gd_{0.75}Sr_{0.2}Ba_{0.05})_{0.2}Ce_{0.8}O_{2-\delta}$ (for un-doped $Gd_{0.2}Ce_{0.8}O_{2-\delta}$ the increase of total conductivity in the presence of hydrogen is 14 times higher in comparison with air and for doped 5 times, while for La and Sm is about 10 times higher for both un-doped and doped compounds). Since the value of total conductivity in hydrogen mainly depends on the level of the n-type electronic conductivity, which appears because of the reduction of Ce^{4+} to Ce^{3+}, probably the introduction of Ba^{2+} and Sr^{2+} into the sublattice of Gd^{3+} decreases the extent of ceria's reduction in this sample in comparison with $Gd_{0.2}Ce_{0.8}O_{2-\delta}$. However, it is very likely that $(Gd_{0.75}Sr_{0.2}Ba_{0.05})_{0.2}Ce_{0.8}O_{2-\delta}$ samples, which have

Table 4
Electrical conductivity of $Ln_{0.2}Ce_{0.8}O_{2-\delta}$ and $(Ln_{0.75}Sr_{0.2}Ba_{0.05})_{0.2}Ce_{0.8}O_{2-\delta}$ (where Ln = Sm, Gd, La) in $H_2 + 3\%H_2O$ at 700, 800, 900 °C and the calculated E_a values of total conductivity (in the temperature range of 600–900 °C)

Composition	$H_2 + 3\%H_2O$, σ_{tot} (S cm^{-1}) 700 °C	$H_2 + 3\%H_2O$, σ_{tot} (S cm^{-1}) 800 °C	$H_2 + 3\%H_2O$, σ_{tot} (S cm^{-1}) 900 °C	$H_2 + 3\%H_2O$, E_a (kJ mol^{-1})
$La_{0.2}Ce_{0.8}O_{2-\delta}$	0.249	0.447	0.703	51
$Sm_{0.2}Ce_{0.8}O_{2-\delta}$	0.418	0.576	0.652	47
$Gd_{0.2}Ce_{0.8}O_{2-\delta}$	0.178	0.529	0.881	76
$(La_{0.75}Sr_{0.2}Ba_{0.05})_{0.2}Ce_{0.8}O_{2-\delta}$	0.451	0.672	0.712	37
$(Sm_{0.75}Sr_{0.2}Ba_{0.05})_{0.2}Ce_{0.8}O_{2-\delta}$	0.514	0.862	1.373	44
$(Gd_{0.75}Sr_{0.2}Ba_{0.05})_{0.2}Ce_{0.8}O_{2-\delta}$	0.220	0.376	0.428	43

the lowest density among the co-doped samples, will undergo the destructive influence of H_2-containing atmosphere more intensively and their conductivity will be lower due to microcracks into the bulk of the samples.

3.3. Effect of oxygen partial pressure

Taking into account that one of the most important requirements for the stable operation of SOFC systems under reducing atmosphere, is the stability of the solid electrolyte, in the present work the dependence of samples' electrical conductivity on different oxygen activities (0.21–10^{-22} atm) at different temperatures (750 and 900 °C) was also investigated. It is well known, that when CeO_2 is reduced to CeO_{2-x}, defects are generated in the form of Ce^{3+}, which in the Kröger-Vink notation is written as Ce'_{Ce}, since Ce^{3+} has one negative charge compared to the normal lattice. It is generally accepted that the main compensating defects in CeO_{2-x} are oxygen vacancies [16]. The process of ceria's reduction may be written as:

$$O_O^{\times} + 2Ce_{Ce}^{\times} \rightarrow \frac{1}{2}O_2 + V_O^{\bullet\bullet} + 2Ce'_{Ce} \quad (5)$$

Assuming that there is no interaction between the various defects (only valid for very low concentrations) the law of mass action is valid. Applied on reaction (5) this gives:

$$[Ce'_{Ce}]^2[V_O^{\bullet\bullet}]P_{O_2}^{1/2} = \text{const} \quad (6)$$

as the concentrations of $O_O^{\times}$ and $Ce_{Ce}^{\times}$ are approximately constant. In the case of un-doped ceria $\lfloor Ce'_{Ce} \rfloor = 2x$ and $\lfloor V_O^{\bullet\bullet} \rfloor = x$. Insertion in reaction (6) and rearrangement gives:

$$x = \text{constant} \times P_{O_2}^{-1/6} \quad (7)$$

Oxygen vacancies may also be introduced by doping with metal oxides with lower valences:

$$Sm_2O_3 \Rightarrow CeO_2 = 2Sm'_{Ce} + 3O_O^{\times} + V_O^{\bullet\bullet} \quad (8)$$

$$O_O^{\times} = V_O^{\bullet\bullet} + 2e' + \frac{1}{2}O_2 \quad (9)$$

For doped ceria the vacancies' concentration may be also regarded as x in the low oxygen partial pressure range and the main charge carriers are Sm'_{Ce}; so taking into account that $\lfloor Sm'_{Ce} \rfloor = 2x$ and $\lfloor V_O^{\bullet\bullet} \rfloor = x$ the exponent is again equal with −1/6:

$$x = \text{constant} \times P_{O_2}^{-1/6} \quad (10)$$

Fig. 3 shows the dependence of CeO_2, $Sm_{0.2}Ce_{0.8}O_{2-\delta}$ and $(Sm_{0.75}Sr_{0.2}Ba_{0.05})_{0.2}Ce_{0.8}O_{2-\delta}$ conductivity on the partial pressure of oxygen at 900 °C. For pure CeO_2 there is no region with constant conductivity. A fitting curve for CeO_{2-x} has a slope of −1/7 in the high oxygen partial pressure range 10^{-7}–0.21 atm. This behavior is not in accordance with the theory (Eq. (7)), probably due to impurities. As a matter of fact, many researchers had difficulties in obtaining n-value of 6 for CeO_2 because of the same reason [16,17]. In the region of intermediate oxygen partial pressures (10^{-12}–10^{-7} atm), the slope

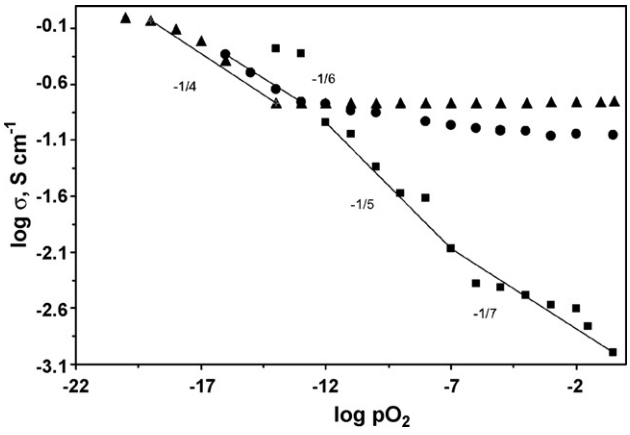

Fig. 3. Dependence of conductivities of CeO_2 (■), $Sm_{0.2}Ce_{0.8}O_{2-\delta}$ (●) and $(Sm_{0.75}Sr_{0.2}Ba_{0.05})_{0.2}Ce_{0.8}O_{2-\delta}$ (▲) on oxygen partial pressure at 900 °C.

changes approximately to −1/5, which is in agreement with the data reported by other authors [17]. This region may be characterized by the predominance of a combination of singly and doubly ionized oxygen vacancies.

In the case of $Sm_{0.2}Ce_{0.8}O_{2-\delta}$, there is a region of the ionic conductivity (10^{-6}–0.21 atm), where conductivity does not depend on P_{O_2} and its value is determined by the doping level. The conductivity increases with the decrease of P_{O_2} with a slope of −1/6 in the intermediate region of the oxygen partial pressures (10^{-16}–10^{-7} atm), which is in agreement with the theory (Eq. (10)). In the case of $(Sm_{0.75}Sr_{0.2}Ba_{0.05})_{0.2}Ce_{0.8}O_{2-\delta}$ one can distinguish three regions: the first one is the ionic conductive region, where conductivity does not depend on the oxygen partial pressure (10^{-14}–0.21 atm), the second one is the mixed conducting region (n-type semi-conductivity and ionic conductivity), where conductivity increases with the decrease of P_{O_2} with a slope equal to −1/4, and the third one is the region where conductivity becomes almost constant again. The third region cannot be described by the theory without taking the interaction between the various defects into account. Probably this effect may be explained by the formation of ordering phases in this compound at low oxygen partial pressures. The ionic conductivity region of $(Sm_{0.75}Sr_{0.2}Ba_{0.05})_{0.2}Ce_{0.8}O_{2-\delta}$ reaches up to 10^{-14} atm in comparison with 10^{-6} for $Sm_{0.2}Ce_{0.8}O_{2-\delta}$, suggesting that the ionic domain of the doped CeO_2-based material with high suggested index is apparently expanded by the enhancement of ionic conductivity, which is in agreement with Mori et al. [5].

At 750 °C the ionic conductivity region for $(Sm_{0.75}Sr_{0.2}Ba_{0.05})_{0.2}Ce_{0.8}O_{2-\delta}$ is extended up to 10^{-21} atm (Fig. 4). The same three regions of the dependence of the logarithm of conductivity on the logarithm of P_{O_2}, are also distinguished in the cases of $(Ln_{0.75}Sr_{0.2}Ba_{0.05})_{0.2}Ce_{0.8}O_{2-\delta}$, Ln = Gd, La, too. The ionic conductivity regions of Gd and La at 750 °C are almost equal up to 10^{-15} and 10^{-16} atm, respectively, and considerably smaller than Sm. This fact is in agreement with the theoretical assumption about the average ionic radius. The existence of the region of constant conductivity for $(Gd_{0.75}Sr_{0.2}Ba_{0.05})_{0.2}Ce_{0.8}O_{2-\delta}$ is not pronounced in the measured region of P_{O_2}, and the fitting curve's

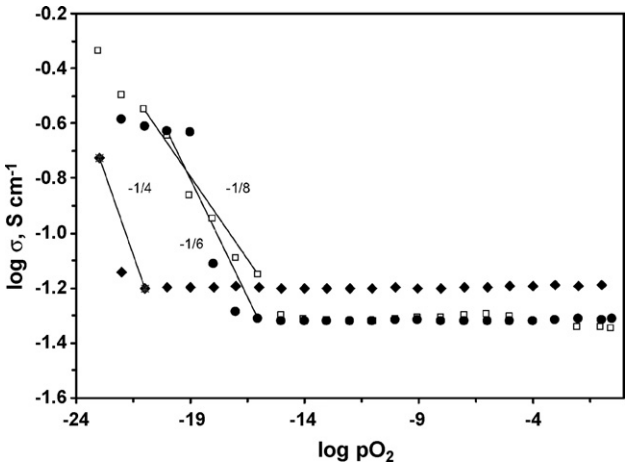

Fig. 4. Dependence of conductivities of $(Gd_{0.75}Sr_{0.2}Ba_{0.05})_{0.2}Ce_{0.8}O_{2-\delta}$ (□), $(La_{0.75}Sr_{0.2}Ba_{0.05})_{0.2}Ce_{0.8}O_{2-\delta}$ (●) and $(Sm_{0.75}Sr_{0.2}Ba_{0.05})_{0.2}Ce_{0.8}O_{2-\delta}$ (♦) on oxygen partial pressure at 750 °C.

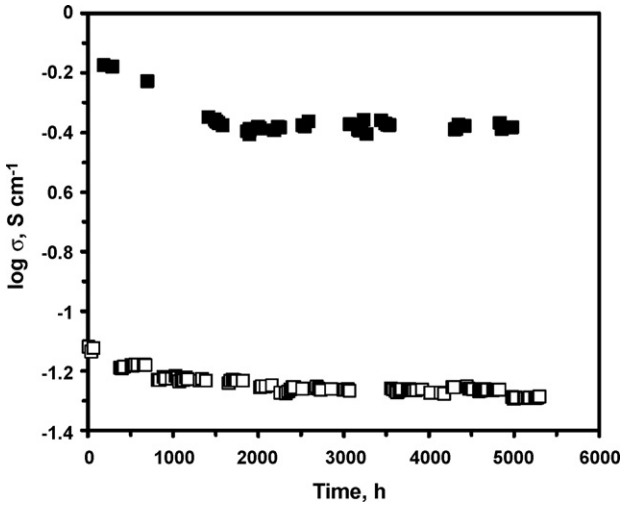

Fig. 5. Total conductivity of $(La_{0.75}Sr_{0.2}Ba_{0.05})_{0.2}Ce_{0.8}O_{2-\delta}$ in air (□) and $H_2 + 3\%H_2O$ (■) at 1073 K as a function of time.

slope in the n-type semi-conductive region is approximately −1/8, while for La and Sm, −1/6 and −1/4, respectively.

The quantitative prediction of the effect of temperature on conductivity (and consequently on the power density) and on the electronic domain boundary (EDB) is required to assess the effective operation temperature range of this new fuel cell electrolyte. The influence of temperature on electronic conductivity was determined by measuring the total conductivity σ_{tot} as a function of P_{O_2} at three temperatures (750, 900 and 1000 °C). The ionic conductivity σ_i was then subtracted to yield σ_{el} versus P_{O_2}. Since the electrolytic areas for $Ln_{0.2}Ce_{0.8}O_{2-\delta}$ and $(Ln_{0.75}Sr_{0.2}Ba_{0.05})_{0.2}Ce_{0.8}O_{2-\delta}$ were too different, in this work the values of σ_{el} at $P_{O_2} = 10^{-15}$ and $P_{O_2} = 10^{-18}$ atm, respectively, were taken into consideration. These data were plotted as $\log \sigma_{el}$ versus $10^3\,T^{-1}$ and from the slope the activation energy was calculated. The values of the activation energy of electronic conductivity, E_{el}, are presented in Table 5. In the case of $Gd_{0.2}Ce_{0.8}O_{2-\delta}$ the obtained E_{el} values are in good agreement with the data reported by Maricle et al. [3]. The introduction of alkaline-earth metals increases significantly E_{el}. This activation energy includes the enthalpy of reduction of the ceria's lattice to generate the electrons, as well as the activation energy for the mobility of the electrons (E_e). However, since E_e is significantly lower than the activation energy of ionic conductivity E_i, and in turn, E_i varies in the narrow range of 62–83 and 58–74 kJ mol^{-1} for $Ln_{0.2}Ce_{0.8}O_{2-\delta}$ and $(Ln_{0.75}Sr_{0.2}Ba_{0.05})_{0.2}Ce_{0.8}O_{2-\delta}$, respectively, the measured activation energy is dominated by the enthalpy of reduction term. For $Gd_{0.2}Ce_{0.8}O_{2-\delta}$ and $(Gd_{.75}Sr_{0.2}Ba_{0.05})_{0.2}Ce_{0.8}O_{2-\delta}$ the obtained values were in good agreement with the ones of Maricle et al. [3]; however, the values of E_{el} for $(Ln_{0.75}Sr_{0.2}Ba_{0.05})_{0.2}Ce_{0.8}O_{2-\delta}$, where Ln = Sm, La, were significantly higher. This indicates that the secondary dopants had stabilized the ceria's lattice against reduction in this case. The electrolytic domain boundary was defined as the P_{O_2}, at which the electronic and ionic conductivities are equal. The values of EDB are presented in Table 5. The reduction of the EBD accomplished by the introduction of Sr and Ba is obvious.

3.4. Long-term stability investigation

Indisputably, for practical applications of ceria-based materials, the investigation of their properties as a function of time, during the exposure at different gas mixtures and at high temperatures, is of great importance. In the present work, the behavior of conductivity during long-term experiments of $(La_{0.75}Sr_{0.2}Ba_{0.05})_{0.2}Ce_{0.8}O_{2-\delta}$ in air and in $H_2 + 3\%H_2O$ is shown in Fig. 5. It was found that in air the total conductivity was smoothly decreasing during the first 95 days of the investigation process – a total decrease by 1.5 times was observed – and

Table 5
Activation energy of electronic conductivity (E_{el}) and EDB values, at different temperatures and oxygen partial pressures

Composition	EDB log pO_2 (atm)		E_{el} (kJ mol^{-1})	
	900 °C	750 °C	$pO_2 = 10^{-15}$ atm	$pO_2 = 10^{-18}$ atm
$La_{0.2}Ce_{0.8}O_{2-\delta}$	−14	−16	190.09	
$Sm_{0.2}Ce_{0.8}O_{2-\delta}$	−9	−12	150.52	
$Gd_{0.2}Ce_{0.8}O_{2-\delta}$	−11	−15	165.96	
$Gd_{0.2}Ce_{0.8}O_{2-\delta}$ [3]		−19 (700 °C)	209.38	
$(La_{0.75}Sr_{0.2}Ba_{0.05})_{0.2}Ce_{0.8}O_{2-\delta}$	−15	−18		229.65
$(Sm_{0.75}Sr_{0.2}Ba_{0.05})_{0.2}Ce_{0.8}O_{2-\delta}$	−16	−18		445.78
$(Gd_{0.75}Sr_{0.2}Ba_{0.05})_{0.2}Ce_{0.8}O_{2-\delta}$	−14	−22		192.02

then it became practically constant. In the case of hydrogen, the conductivity was sharply decreased by 2 times during the first 79 days of the investigation process, while afterwards it became constant too.

The process of aging in solid oxide electrolytes, which results in the decrease of electrical conductivity after long-term annealing, has been extensively studied for doped zirconia ceramics [18,19]. The possible causes of aging presented in literature are the following: (i) the precipitation of long-range ordered phases such as $Y_2Zr_2O_7$, (ii) the formation and the precipitation of tetragonal phase in the cubic grains, (iii) the segregation of the dopant-rich layer near the grain boundaries and triple points and (iv) the trapping of oxygen vacancies toward dopant cations with time due to the coulombic force (i.e., short range ordering of oxygen vacancies) [20]. However, there is no adequate information about aging behavior of ceria-based electrolytes. It was found that the aging behavior of doped ceria cannot be explained using the aging mechanisms applied to the doped zirconia.

The aging process in $Ln_xCe_{1-x}O_{2-\delta}$ (Ln = La, Gd, Sm) was explained by the formation of micro-domains, which leads to a conductivity decrease as they prevent oxygen vacancies' passing through the lattice [21]. In the work of Zhang et al. [20] it was found that the critical dopant concentration at which the micro-domains start to form, is $x = 0.15$ for La-doped ceria. Below this concentration conductivity is governed only by the association enthalpy, while above the critical dopant concentration conductivity is determined mainly by the micro-domains rather than the association enthalpy. Since in our case the dopant concentration is above the critical one, the aging behavior may be explained by the formation of micro-domains. In addition, the decrease of total conductivity can be explained by the decrease in the grain boundary conductivity, because of the segregation of dopand-rich layers near the grain boundaries as a result of long-term annealing.

4. Conclusions

In the present work the structural and electrical properties of $Ln_{0.2}Ce_{0.8}O_{2-\delta}$ (where Ln = Sm, La, Gd) solid solutions doped with small amounts of Sr and Ba were investigated. It was found that the dopants, as alkali-earth elements, are completely dissolved in the fluorite CeO_2 lattice resulting in the increase of the parameters of the elementary cell. The introduction of alkaline-earth metals enhances the sintering properties of $Ln_{0.2}Ce_{0.8}O_{2-\delta}$ and increases samples' conductivity, decreasing at the same time the activation energy of total conductivity in air. It is clear from the results of the conductivity measurements versus P_{O_2} that the reduction of Ce^{4+} in a fluorite lattice is inhibited by the expansion of the CeO_2 lattice. Furthermore, the highest values of conductivity and the lowest electrolytic domain boundary, with very low value of activation energy, are obtained in the case of $(Sm_{0.75}Sr_{0.2}Ba_{0.05})_{0.2}Ce_{0.8}O_{2-\delta}$. Finally, the $(Ln_{0.75}Sr_{0.2}Ba_{0.05})_{0.2}Ce_{0.8}O_{2-\delta}$ samples, where Ln = La, Gd were found to be quite effective in suppressing the reduction of CeO_2.

References

[1] T.H. Etsell, S.N. Flengas, Chem. Rev. 70 (1970) 339–376.
[2] A. Yan, V. Maragou, A. Arico, M. Cheng, P. Tsiakaras, Appl. Catal. B: Environ. 76 (2007) 320–327.
[3] D.L. Maricle, T.E. Swarr, S. Karavolis, Solid State Ionics 52 (1992) 173–182.
[4] N. Kim, B. Kim, D. Lee, J. Power Sources 90 (2000) 139–143.
[5] T. Mori, J. Drennan, Y. Wang, J. Li, T. Ikegami, J. Therm. Anal. Calorim. 70 (2002) 309–319.
[6] T. Mori, H. Yamamura, J. Mater. Synth. Process. 6 (1998) 175–179.
[7] R.D. Shannon, C.T. Prewitt, Acta Crystallogr. B 25 (1969) 925–946.
[8] J.A. Kilner, Solid State Ionics 129 (2000) 13–23.
[9] H.M. Rietveld, J. Appl. Cryst 2 (1969) 65–71.
[10] H. Hayashi, M. Kanoh, C. Quan, H. Inaba, S. Wang, M. Dokiya, H. Tagawa, Solid State Ionics 132 (2000) 227–233.
[11] V.V. Kharton, F.M.B. Marques, A. Atkinson, Solid State Ionics 174 (2004) 135–149.
[12] M. Gödickemeier, Mixed ionic electronic conductors for solid oxide fuel cells, PhD Thesis No. 11348, Swiss Federal Institute of Technology, ETH Zurich, 1996.
[13] S. Sameshima, T. Ichikawa, M. Kawaminami, Y. Hirata, Mater. Chem. Phys. 61 (1999) 31–35.
[14] E. Suda, B. Pacaud, M. Mori, J. Alloys Compd. 408–412 (2006) 1161–1164.
[15] H. Yahiro, K. Eguchi, H. Arai, Solid State Ionics 36 (1989) 71–75.
[16] M. Mogensen, N.M. Sammes, G.A. Tompsett, Solid State Ionics 129 (2000) 63–94.
[17] R.N. Blumental, P.W. Lee, R.J. Panlener, J. Electrochem. Soc. 118 (1971) 123–129.
[18] A.N. Vlasov, M.V. Perfiliev, Solid State Ionics 25 (1987) 245–253.
[19] S.P.S. Badwal, Solid State Ionics 52 (1992) 23–32.
[20] T.S. Zhang, J. Ma, L.B. Kong, S.H. Chan, J.A. Kilner, Solid State Ionics 170 (2004) 209–217.
[21] T. Mori, J. Drennan, J.H. Lee, J.G. Li, T. Ikegami, Solid State Ionics 154–155 (2002) 461–466.